Highly accurate transition frequencies in the H_2 Lyman and Werner absorption bands[1]

J. Philip, J.P. Sprengers, Th. Pielage, C.A. de Lange, W. Ubachs, and E. Reinhold

Abstract: The transition frequencies of low-J excitation lines in the $B^1\Sigma_u^+ - X^1\Sigma_g^+$, $(v', 0)$ Lyman bands have been measured for $v' = 2$–18 and in the $C^1\Pi_u - X^1\Sigma_g^+$, $(v', 0)$ Werner bands for $v' = 0$–4, using a narrow-band tunable extreme UV laser source at wavelengths $\lambda = 92$–105 nm in conjunction with the technique of $1 + 1'$ two-photon ionization. The measurements can be divided into three categories for which varying absolute accuracies were obtained. Special focus was on the B, $v' = 2$–5 bands, where an accuracy of 0.004 cm^{-1} or $\delta\nu/\nu = 4 \times 10^{-8}$ is achieved. For transitions to B, $v' \leq 13$ and C, $v' \leq 3$ states the accuracy is 0.005 cm^{-1} or $\delta\nu/\nu = 5 \times 10^{-8}$. Due to a different frequency mixing scheme uncertainties for B, $v' \geq 13$ and C, $v' = 4$ are at the level of 0.011 cm^{-1} or $\delta\nu/\nu = 1.1 \times 10^{-7}$. Inspection of combination differences between R(J) and P($J + 2$) lines shows that the accuracies are even better than estimated in the error budget. Based on the measurements of 138 spectral lines and the known combination differences, transition frequencies of 60 P-lines could be calculated as well, so that a data base of 198 accurately calibrated lines results for the Lyman and Werner bands of H_2.

Key words: vacuum UV, molecular spectroscopy, hydrogen, precision metrology.

Résumé : On a mesuré les fréquences de transition des raies d'excitation de faible J dans les bandes de Lyman $B^1\Sigma_u^+ - X^1\Sigma_g^+$, $(\nu', 0)$, pour des valeurs de ν' allant de 2 à 18 ainsi que dans les bandes de Werner $C^1\Pi_u - X^1\Sigma_g^+$, $(\nu', 0)$, pour des valeurs de ν' allant de 0 à 4 en faisant appel à une source laser UV extrême, ajustable et à bande mince, à des longueurs d'onde, λ, allant de 92 à 105 nm, utilisée de concert avec la technique d'ionisation à deux photons $1 + 1'$. Les mesures peuvent être divisées en trois catégories qui diffèrent entre elles par la précision des mesures obtenues. On a concentré nos efforts sur les bandes B, $\nu' = 2$–5, pour lesquelles la précision a été de 0,004 cm^{-1} ou $\delta\nu/\nu = 4 \times 10^{-8}$. Pour les transitions vers B, $\nu' \leq 13$ et C, $\nu' \leq 3$, la précision est de 0,005 cm^{-1} ou $\delta\nu/\nu = 5 \times 10^{-8}$. En raison d'une méthode différente de combinaison des fréquences, les incertitudes associées à B, $\nu' \geq 13$ et C, $\nu' = 4$, le niveau de précision est de 0,011 cm^{-1} ou $\delta\nu/\nu = 1{,}1 \times 10^{-7}$. Un examen des différences des combinaisons entre les raies R(J) et P($J + 2$) montre que les précisions sont meilleures que celles évaluées dans le budget des erreurs. Sur la base de mesures de 138 raies spectrales et de différences de combinaison connues, on a pu aussi calculer les fréquences de transition de 60 raies P et il en résulte qu'une base de données de 198 raies bien calibrées est disponible pour les bandes de Lyman et de Werner du H_2.

Mots clés : UV lointain, spectroscopie moléculaire, hydrogène, métrologie de précision.

[Traduit par la Rédaction]

1. Introduction

Molecular hydrogen is the smallest neutral molecule and the most abundant molecular species in the universe. The Lyman bands, corresponding to the $B^1\Sigma_u^+ - X^1\Sigma_g^+$ system, and the Werner bands, corresponding to the $C^1\Pi_u - X^1\Sigma_g^+$ system, connect the electronic ground state to the lowest excited states of singlet and *ungerade* symmetry in a dipole-allowed transition, making them the most prominent features in the H_2-spectrum. Both systems relate to the $1s$–$2p$ resonance line of the H_2 molecule in analogy to the Lyman-α line in the H atom. In case of the $B^1\Sigma_u^+$ state the electron is promoted to a $2p\sigma$ orbital, whereas for the $C^1\Pi_u$ state the electron is in $2p\pi$. In his pioneering studies on the vacuum UV emission spectrum, now a century ago, Lyman was the first to positively assign a spectrum to the H_2 molecule (1, 2): the $B^1\Sigma_u^+ - X^1\Sigma_g^+$ system. Later, in 1926, Werner was the first to assign spectral lines pertaining to the $C^1\Pi_u - X^1\Sigma_g^+$ system (3). Dr. Herzberg, to whom we dedicate the present study, devoted an appreciable part of his career to the study of the spectrum of molecular hydrogen. Among his pioneering breakthroughs we mention the observation of the IR quadrupole spectrum (4), his analysis of the Rydberg spectrum, with Jungen (5), laying the foundations for the application of quantum defect theory in molecules, the determination of the dissociation energy (6), and his work with Jungen, Dabrowski, and Vervloet (7) on the measurement of IR inter-Rydberg transitions, leading to a determination of the ionization potential. Also, for the Lyman and Werner bands Herzberg made cru-

Received 3 October 2003. Published on the NRC Research Press Web site at http://canjchem.nrc.ca/ on 10 June 2004.

J. Philip, J.P. Sprengers, Th. Pielage, C.A. de Lange, and W. Ubachs.[2] Laser Centre, Department of Physics and Astronomy, Vrije Universiteit, Amsterdam, Netherlands.
E. Reinhold. Laboratoire Aimé Cotton, Campus d'Orsay, Université Paris-Sud, Orsay, France.

[1]This article is part of a Special Issue dedicated to the memory of Professor Gerhard Herzberg.

[2]Corresponding author (e-mail: wimu@nat.vu.nl).

 doi: 10.1139/V04-042

cial contributions, with Howe (8) and with Dabrowski (9), on a full rotational analysis of the emission spectra. High resolution absorption spectra of the Lyman and Werner band systems, using classical grating spectrometers, were investigated by Namioka (10) and by Dabrowski (11). The classical studies culminated in a comprehensive study of the H_2 VUV-spectrum by scientists at the Meudon Observatory, which was published in the form of a high-resolution spectroscopic atlas (12).

Developments on the experimental side were, over the years, accompanied by theoretical studies, for which the H_2 molecule is a benchmark system. Ab initio calculations of the potential energy curves have been produced using the Born–Oppenheimer approximation and calculating separately the mass-dependent adiabatic corrections to the potential curves as well as the non-adiabatic corrections for determination of accurate level energies. Advanced calculations for the $X^1\Sigma_g^+$ electronic ground state are those of Wolniewicz (13). An accurate potential energy curve for the $B^1\Sigma_u^+$ state was reported by Cencek et al. (14) and for the $C^1\Pi_u$ state by Wolniewicz (15). For a calculation of level energies in the $B^1\Sigma_u^+$ and $C^1\Pi_u$ excited states the couplings between the $B^1\Sigma_u^+$, $B'^1\Sigma_u^+$, $C^1\Pi_u$, and $D^1\Pi_u$ states and the resulting interferences have to be treated, based upon the input of ab initio potentials. The Meudon group has calculated those coupling effects in a number of studies of increasing accuracy (16) finally resulting in tables of transition frequencies for the Lyman bands (17) and Werner bands (18). Based upon these studies, a vast amount of rotationally resolved lines of the H_2 atlas (12) could be assigned.

The first observation of molecular hydrogen in space was performed with a rocket-borne spectrometer detecting Lyman band absorption in the optical path toward ξ Persei (19). Since then various satellite-based telescopes including spectrometers in the vacuum UV range have been launched for the study of H_2 and other molecules. The *Copernicus* satellite telescope (20) was in operation for many years, while the better resolving instruments ORFEUS and IMAPS were flown aboard the Space Shuttle for limited periods. The Hubble Space Telescope yielded a greatly improved sensitivity combined with a good resolving power and absorption from H_2 vibrationally excited levels could even be recorded (21). The *Galileo* orbiter, equipped with an UV (113–432 nm) as well as an extreme-UV (54–128 nm) spectrometer, recorded the Lyman and other H_2 bands from the north and south polar regions of Jupiter (22). Since June 1999, the Far ultraviolet spectroscopic explorer (FUSE) is in flight and detecting hydrogen in space. It covers the wavelength range 90.5–118.7 nm, the range of the strong Lyman and Werner absorption bands, with high resolution (23) and with a 10^4 greater sensitivity than Copernicus.

The present paper reports on a high-resolution laser spectroscopic study of the Lyman and Werner bands. A narrow-band tunable extreme ultraviolet (XUV) laser source is used in a $1 + 1'$ resonance-enhanced multi-photon ionization (REMPI) scheme to determine transition frequencies of various low-J lines in $B^1\Sigma_u^+ - X^1\Sigma_g^+(v', 0)$ bands for $v' = 2$–18 and in $C^1\Pi_u - X^1\Sigma_g^+(v', 0)$ bands for $v' = 0$–4. In previous high-resolution studies by our group, a coherent laser-based XUV-source was also used, but now the resolution has been increased by an order of magnitude, while at the same time the methods for absolute calibration have been improved. Initially, in a pilot study, the $B–X(10, 0)$ band had been studied (24). This work was extended to a comprehensive laser excitation study of 291 lines in Lyman $B–X(v', 0)$ bands for $v' = 10$–19 and Werner $C–X(v', 0)$ bands for $v' = 0$–5 (25). Later, a further extension was performed for $B–X(v', 0)$ bands for $v' = 20, 22, 23, 25$–27, and $C–X(v', 0)$ bands for $v' = 6$–10 (26). The absolute accuracies on the transition frequencies in these laser-based measurements varied between 0.02 and 0.06 cm^{-1}. These accuracies have been improved now by almost an order of magnitude.

2. Experiment and assessment of error budget

The Amsterdam narrow-band tunable XUV radiation source and its application in atomic (27) and molecular (28) spectroscopy have been described previously. A schematic layout of two slightly differing experimental setups, further referred to as schemes I and II, are displayed in Fig. 1. In short, the radiation source consists of a tunable ring-dye-laser delivering continuous wave (cw) radiation in the range 570–660 nm, a three-stage pulsed-dye amplifier (PDA) pumped by a pulsed Nd:YAG laser, a frequency-doubling crystal for converting the visible output of the PDA to the UV range, and a pulsed gas jet in which the pulsed UV radiation is frequency-tripled to cover the wavelength range 95–110 nm. The bandwidth of the XUV light in this range was previously estimated at 250–300 MHz, slightly below 0.01 cm^{-1} (see also ref. 28). The pulsed-XUV beam is crossed perpendicularly by a molecular beam obtained from a pulsed nozzle. In the interaction zone signal is generated by $1 + 1'$ photo-ionization, whenever the XUV radiation is tuned in resonance with a Lyman or Werner absorption line. In view of the cooling effect of the pulsed molecular beam, only transitions originating in the low rotational levels can be accessed. Spectral lines are recorded by scanning the cw laser system and monitoring the H_2^+-ion production in the interaction zone. The wavelength used in the ionizing step is the UV wavelength before tripling, corresponding to $\lambda_{UV} = 3\lambda_{XUV}$ at each H_2 resonance. For the $B–X(2, 0)$ band the total energy of the XUV and UV photons is not sufficient to produce H_2^+ ions directly. Nevertheless, this band could be recorded from the signal induced by a $1 + 2'$ process using the region of high Rydberg states for resonance enhancement. In this case, the H^+ signal was monitored, which originates from photo-dissociated H_2 molecules, producing $H(n = 2)$ atoms that are subsequently ionized. The $B–X$ (0,0) and (1,0) bands were not covered in this study because the saturation I_2 standard does not extend to these wavelengths for the fundamental (29, 30).

At the short wavelength limit (at $\lambda < 570$ nm), problems arose with the operation of the cw ring-dye laser, which was pumped by a Millennia 5W laser at 532 nm. Hence, the study was limited to $B(v' \leq 13)$ and $C(v' \leq 3)$ when using scheme I as displayed in Fig. 1. For this reason, wavelengths in the range $\lambda < 95$ nm were produced via an alternative frequency mixing scheme (shown as scheme II in Fig. 1). The green output of the Nd:YAG laser was used, both for pumping the PDA as well as for sum-frequency mixing with the output of the PDA, to reach shorter wavelengths. These methods have been described in more detail in a separate paper (31). Although the output frequency of the Nd:YAG laser is in principle fixed, temperature drifts caused slowly varying frequency excursions of several

Fig. 1. Schematic layout of the experimental setup for both schemes used.

(*a*) Scheme I

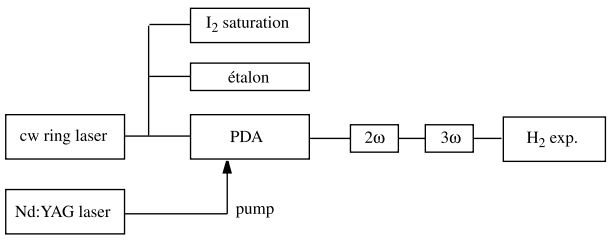

(*b*) Scheme II

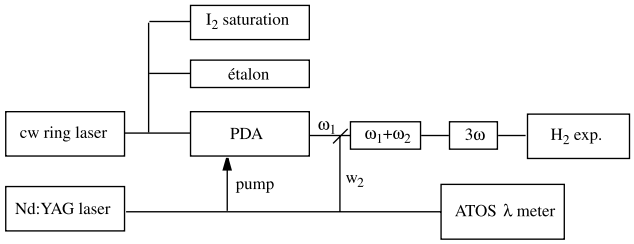

GHz during a measurement session. Its frequency was therefore monitored on-line by a four-étalon wavelength meter (ATOS), which was calibrated on an absolute scale by comparison to I_2 saturated lines, during each measurement session. This method yields an absolute accuracy of 100 MHz for the Nd:YAG output at 18 788 cm^{-1}.

The linewidths observed in the recording of the Lyman and Werner lines are ≈500 MHz, and slightly dependent on the measurement geometry and molecular beam conditions chosen. The bandwidth of the XUV laser source of ≈300 MHz (see refs. (27, 28)) is independent of the choice of scheme I or II. The upper $B^1\Sigma_u^+$ and $C^1\Pi_u$ states have lifetimes of 0.5–1 ns causing a Lorentzian type broadening of up to 300 MHz. For experimental geometries in which the nozzle–skimmer distance in the molecular beam was set at 15 cm (typical measurement conditions), the Doppler contribution was found to be negligible, particularly for molecular beams in which 25% H_2 was seeded in krypton gas to lower the average velocity of the molecules. Additional broadening was found if the nozzle–skimmer distance was lowered (i.e., when the signal intensity had to be increased). At very short nozzle–skimmer distances, we found increased population of high rotational states ($J = 4$ and $J = 5$), possibly due to glancing collisions at the conical skimmer surface. Detailed studies were performed comparing the transition frequencies and their Doppler shifts on the nearby lying transitions B–$X(12, 0)$ R(1) in H_2 and $4p^6\,{}^1S$–$5d_{1/2}(J = 1)$ in ^{84}Kr, at various beam conditions (i.e., beam velocities and nozzle–skimmer distances). From these measurements an estimate was made of the Doppler shift and of its effect on the uncertainty of the transition frequencies. The latter is included in the error budget for an amount of 60 MHz. For the set of measurements on B–$X(v', 0)$, $v' = 2$–5 lines an even more careful analysis of the Doppler shift, involving seeding H_2 gas in xenon, yields a maximal systematic error of only 40 MHz.

Calibration of the source was performed by reference measurements with the visible output of the cw ring-dye laser. Simultaneously with the H_2 spectrum, transmission fringes of a pressure- and temperature-stabilized étalon and the saturation spectrum of molecular iodine were recorded. The free spectral range (FSR) of the étalon was well calibrated at 148.9567 MHz and the t-hyperfine components of the I_2 saturation spectrum were calibrated in our laboratory with an absolute accuracy (2σ) of 2 MHz (29, 30). Hence, the XUV frequency scale can be obtained by multiplication of the scale for visible frequencies by a factor of six (i.e. for scheme I in Fig. 1), thus accounting for frequency doubling and subsequent frequency tripling. Estimates were made of the uncertainty caused by frequency drift of the pressure- and temperature-stabilized étalon. In the most unfortunate cases, when useful I_2 saturation lines were far away, continuous scans of ≈ 20 min duration had to be recorded, resulting in contributions to the error budget of 20 MHz (scheme I) or 10 MHz (scheme II). Special precautions were taken during measurements of the B–$X(v', 0)$ Lyman bands for $v' = 2$–5. During these recordings the étalon was actively stabilized with the aid of a HeNe laser, which was itself frequency-locked to an I_2 saturation line.

Two examples are presented of spectral recordings of the H_2 spectrum that elucidate the high-resolution capabilities of the setup. Fig. 2 shows the R(0) and R(1) lines in the C–$X(1, 0)$ Werner band, clearly separated by 1.09 cm^{-1}; in the classical absorption spectrum these lines were determined at a separation of 2 cm^{-1}, most likely because of partial overlap (9). A second spectrum, displayed in Fig. 3, shows the nearby lying P(3) line of the C–$X(1, 0)$ band and the R(0) line of the B–$X(9, 0)$ band, separated by only 0.16 cm^{-1}. Recordings of H_2^+ and H^+ signals show that excitation of Werner lines usually yields only parent ions, while excitation of Lyman lines also produces a H^+ signal. Absolute calibration is performed with respect to the t-component of the P(126) line of the B–$X(15, 2)$ band in iodine. Computerized fitting procedures to the spectral lineshapes aid in determining the line centers with high precision. The contribution of the uncertainty of the reference spectrum is minor (10 MHz). A statistical uncertainty in the determination of line centers is caused by the fitting of the observed line profiles. Slight variations in the central frequencies obtained in repeated scans of a transition are also treated as statistical uncertainty. The final value for a line position is obtained by the weighted mean deduced line centers from all scans, using the number of laser pulses per wavelength interval as a weight factor. In this procedure a final statistical uncertainty is derived. For ease of representation, and to take a conservative estimate, an upper limit of the statistical uncertainty in each of the measurement schemes is used, instead of slightly different values for each line. For the very weak lines, and the lines recorded under conditions of additional broadening, a higher estimate of the uncertainty is listed in the Tables. Most lines were recorded three times, except for the set of Lyman bands B–$X(v', 0)$ for $v' = 2$–5, where the lines were recorded 10 or more times. In cases where frequency-mixing scheme II was employed, the calibration uncertainty was dominated by the frequency measurement of the green output of the Nd:YAG laser. Since $\omega_{XUV} = 3\omega_{PDA} + 3\omega_{Nd:YAG}$, the uncertainty of this measurement comes into the error budget three times (i.e., 300 MHz).

The AC-Stark effect in the H_2 Lyman bands was investigated recently by Wetzig et al. (32). The intensity of the XUV beam

Fig. 2. Recording of the R(0) and R(1) lines of the $C–X(1, 0)$ Werner band separated by 1.09 cm^{-1}.

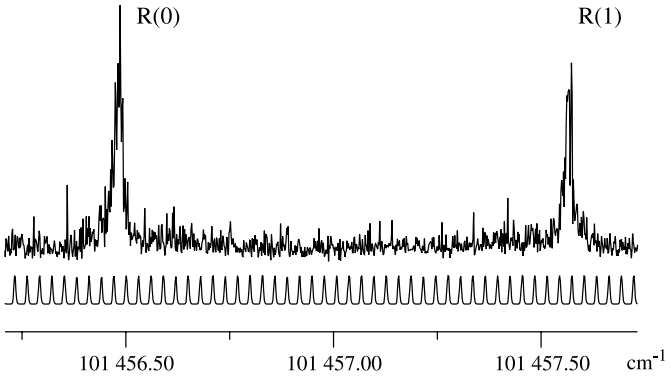

Fig. 3. Recording of the P(3) line of the $C–X(1, 0)$ Werner band and the R(0) line of the $B–X(9, 0)$ Lyman band of H_2 for both the H_2^+ and H^+ signals in the XUV domain. Below: simultaneous recordings of transmission fringes of the stabilized étalon and the saturation spectrum of molecular iodine at the fundamental frequency ($\nu_{XUV}/6$). The line marked with an asterisk denotes the P(126) line in the $B–X(15, 2)$ at 16 811.7958 cm^{-1}.

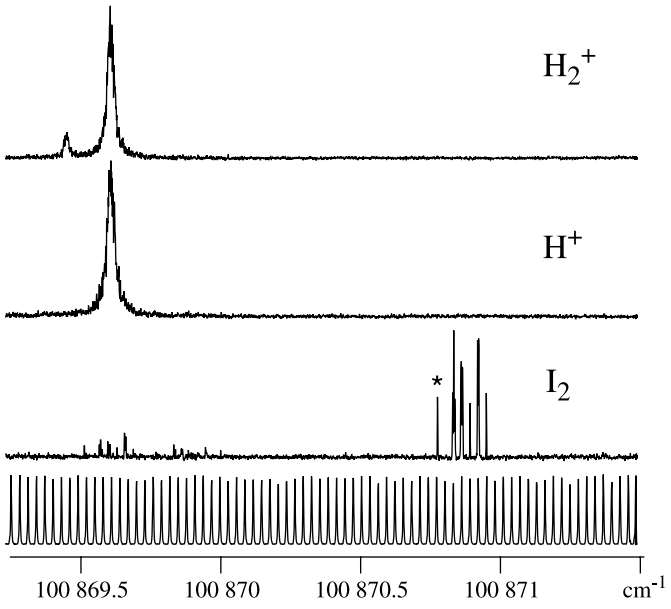

in the present experiment is so low (sub-nJ pulse energies in a diverging beam) that its AC-Stark inducing effects may be neglected, and the UV-ionizing laser in the $1 + 1'$ two-photon ionization process dominates the AC-Stark shifts. The maximum UV intensity in the interaction zone is 4 MW/cm^2 (20 mJ/pulse, 5 ns pulse duration, 1 cm^2 area) at the highest pulse energies used. By taking into account the quadratic Stark effect for $^1\Sigma$ states and the polarizabilities for the $B\,^1\Sigma_u^+$ state as calculated by Rychlewski et al. (33), as well as effective polarizabilities obtained from experimental data, they estimate for the case of $1 + 1'$ REMPI (UV intensities of $I = 10$ GW/cm^2 and parallel polarizations of XUV and UV beams, asymmetrically shaped lines with an intensity maximum shifted by -4.0 cm^{-1}, and a shift of the effective line center by -3.0 cm^{-1}. The polarizability of the $X\,^1\Sigma_g^+$ ground state is orders of magnitude smaller and can be neglected. With the estimated polarizability of ref. 32, this yields a shift of 0.0015 cm^{-1} or less for the line center at the highest pulse energies used in the present study. The work of Wetzig et al. (32), dealing with the $B\,^1\Sigma_u^+$, $v' = 3$ and $v' = 4$ levels, provides an exemplary case. If their analysis may be taken as a guidance, this would result in an upper limit of 50 MHz for the AC-Stark shift for spectral lines recorded at the highest laser pulse energies. In the case of frequency mixing scheme II, lower laser pulse energies (< 10 mJ/pulse) were produced, and hence limits to the AC-Stark shift could be relaxed accordingly. Eikema et al. (27) performed measurements on the $1 + 1'$ REMPI excitation mechanism via the $(2p)\,^1P$ state in He; such a scheme can be considered to represent the unified-atom limit to excitation via $(2p\sigma)$ and $(2p\pi)$ in the H_2 Lyman and Werner bands. From the study on He an AC-Stark shift of 2.5 MHz per MW/cm^2 can be deduced, confirming the estimate on an upper limit for the AC-Stark effect of less than 50 MHz.

In addition to these estimates, an experimental assessment was made of the AC-Stark effect. A large set of over 30 recordings was taken for the R(1) line of the $C–X(1, 0)$ Werner band in a pulse energy range of 2–15 mJ/pulse. From an analysis of these data it follows that a possible AC-Stark shift is smaller than the statistical spread in the data set; no intensity-dependent trend is observed. From these data we conclude that the estimated contribution of 50 MHz to the AC-Stark shift is conservative. In the study of the $B–X(v', 0)$ bands for $v' = 2$–5 another large data set was gathered focusing on laser intensity effects in the range of pulse energies 2–5 mJ/pulse. Even though the statistical error was smaller, no systematic trend that might possibly be attributed to an AC-Stark effect was found; for this particular data set the estimate of the error contribution by the AC-Stark effect is taken at the lower value of 30 MHz.

Two final remarks can be made on perturbing influences of the AC-Stark effect in the present absolute frequency measurements. If the total energy in the $1 + 1'$ REMPI scheme accidentally hits a resonance in the autoionization continuum, the AC-Stark effect may be enhanced, resulting in a possibly larger shift of the observed resonance in the Lyman or Werner bands. Such phenomena might be verified by using a wavelength-tunable ionization laser, but the procedures are too elaborate for addressing all lines in the present data set. Hence, it is not excluded that one or more of the lines undergoes an enhanced AC-Stark effect and the uncertainty in the transition frequency is then larger than specified. However, in the consistency checks (see next section) no such enhanced shifts were found. Secondly, AC-Stark effects on spectral lines induce asymmetric profiles (see e.g., ref. 32), due to splitting of m_J components. No such signatures were observed.

As was discussed in previous studies using the PDA-based narrow-band XUV source, frequency chirp (i.e., frequency excursions during the laser pulses of 5 ns duration as a result of time-dependent gain in the dye amplifiers) form a major limitation in precision studies involving pulsed lasers (27, 34). Although it was demonstrated that the chirp effect, giving rise to a net shift between the center frequency of the pulsed output of the PDA with respect to the cw-laser output (27), can be actively compensated, the procedures to do so are too cumbersome to apply in a study of 70 spectral lines. From the same studies it followed, however, that the chirp effect in a PDA-based XUV

Table 1. Error budget for the transition frequencies in the present high-precision 1 XUV + 1 UV two-photon ionization spectroscopic study in H_2.

Source	Scheme I	Ia	Scheme II
Doppler	60	40	60
AC Stark	50	30	30
Chirp	100	100	70
I_2 calibration	10	10	10
Etalon drift	20	—	10
Nd:YAG calibration	—	—	300
Statistical	80	30	80
Total	152	117	326

Note: The columns under scheme I and scheme II refer to the experimental configurations as shown in Fig. 1, where the data under Ia specifically denote transitions to the $B^1\Sigma_u^+$, $v' = 2$–5 states, where special care was taken to further reduce the uncertainties. All values are given in MHz.

source is limited to systematic shifts of 100 MHz, for the center frequency determined in a $1 + 1'$ two-photon ionization experiment. We adopt this value as an upper limit in the error budget (Table 1). It should be noted that, while this shift is systematic, there is a distribution of chirp shifts over the spectral lines measured in this study. As discussed in refs. 27 and 34, the systematic shift varies and changes sign when tuning a PDA over a single-dye curve; in the present study, full tuning curves of a number of different dyes and dye mixtures were used. For these reasons the chirp contribution to the error budget may be treated as a statistical summation of independent errors.

The contributions to the error budget are given in Table 1 for mixing schemes I and II. The separate column Ia relates to measurements of lines in B–$X(v', 0)$ Lyman bands for $v' = 2$–5, where special caution was taken to minimize some of the contributing causes of uncertainty, while using the measurement geometry of scheme I. For the major fraction of spectral lines this uncertainty was adopted in the list of resulting transition frequencies displayed in the tables. Some of the lines gave larger statistical uncertainties or were measured at unfavorable conditions (low intensity or very short nozzle–skimmer distance); the estimated uncertainties for these lines are indicated in the tables. Particularly in the wavelength range near 615 nm, problems were encountered in running the PDA laser system. As a result only weak signals could be observed in a geometrical configuration with a small nozzle–skimmer distance; the uncertainties in the transition frequencies are therefore higher.

In the measurements performed with scheme I, the frequency chirp in the PDA is the determining factor in the error budget, while in the measurements using scheme II, the uncertainty in the Nd:YAG frequency outweighs other error contributions. In the best case the uncertainty in the absolute frequency corresponds to 1/3 of the line width, while in the other cases it amounts to 2/3 of the line width of the observed resonances.

3. Results, discussion and conclusion

The data on the experimental transition frequencies are arranged in five tables. In Tables 2 and 3 transition frequencies in the H_2 Lyman bands for $v' = 2$–5 and $v' = 6$–13 as obtained with mixing scheme I are presented. Table 4 presents the Lyman lines for $v' = 14$–18, obtained with mixing scheme II. Finally, the transition frequencies of the Werner bands obtained in mixing schemes I and II are listed in Tables 5 and 6. The fact that the study is limited to transitions originating in low J levels is inherently connected to the use of a molecular beam, necessary to enter the regime of sub-Doppler accuracy.

Table 2. Observed transitions of the $B^1\Sigma_u^+ - X^1\Sigma_g^+(v', 0)$ Lyman bands in H_2 for $v' = 2$–5, obtained with frequency mixing scheme I.

J	P(J)	Δ_{o-m}	Band	R(J)	Δ_{o-m}
			(2,0)		
0				92 838.551(4)	−0.029
1	92 684.808(4)	−0.065		92 790.293(4)	−0.090
2				92 659.092(4)	0.075
			(3,0)		
0				94 083.809(4)	−0.011
1	93 931.518(4)	−0.055		94 032.673(4)	−0.070
2	93 729.437(4)	−0.010		93 897.171(4)	0.014
3				93 678.697(4)	−0.044
			(4,0)		
0				95 295.505(4)	−0.015
1	95 144.534(4)	−0.079		95 241.745(4)	−0.048
2				95 102.364(4)	0.017
3				94 878.812(4)	−0.069
			(5,0)		
0				96 474.270(4)	−0.010
1	96 324.532(4)	−0.031		96 418.076(4)	−0.087
2				96 275.091(4)	−0.016
3				96 046.817(4)	−0.054

Note: For this set of measurements the étalon was actively locked to a stabilized HeNe laser, while the Doppler effect was assessed through a number of experiments. The values between parentheses are the uncertainties of the last digits. The transition energies are compared with the experimental values by the Meudon group (Δ_{o-m}) (16).

A first comparison can be made with the classical data of Dabrowski and Herzberg (9), in which an accuracy of 0.15 cm^{-1} is claimed; we find that the data of ref. 9 are on average higher by 0.2 cm^{-1}, with a standard deviation of $\sigma = 0.4$ cm^{-1}. In the tables, the transition frequencies are compared with those of the most accurate values in the literature. On the one hand those are the values of the Meudon group, where we have not adopted the values obtained in direct measurements, as given in the Lyman (17) and Werner tables (18), but rather the experimentally deduced values of the level energies, which relate to an average over emission lines in various bands (16). We converted these values into transition frequencies of the Lyman and Werner bands by adding the most accurate values for the level energies of $X^1\Sigma_g^+$, $v" = 0$ rotational states (36). The transition frequencies of the Meudon analysis are found to be higher by 0.06 cm^{-1} on average, with some scatter that has a standard deviation of 0.047 cm^{-1}. Based on the latter one would expect that the average deviation of our entire data set from the Meudon data is on the order of 0.008 cm^{-1}. This implies that the difference of 0.06 cm^{-1} must be interpreted as a systematic shift. This is not disturbing since in the Meudon analysis an accuracy of 0.15 cm^{-1} is claimed, part of which may be systematic. In measurements of a classical spectrum, the calibration by reference lines is performed for the entire data set

Table 3. Observed transitions of the $B^1\Sigma_u^+ - X^1\Sigma_g^+(v',0)$ Lyman bands in H_2 for $v' = 6$–13, obtained with frequency mixing scheme I.

J	P(J)	Δ_{o-m}	Δ_{o-h}	Band	R(J)	Δ_{o-m}	Δ_{o-h}
				(6,0)			
0					97 620.600(8)	−0.050	
1	97 472.046(8)	−0.087			97 562.127(8)	−0.086	
				(7,0)			
0					98 734.907(5)	−0.003	
1	98 587.513(5)	−0.050			98 674.115(5)	−0.058	
2					98 524.415(6)	−0.012	
				(8,0)			
0					99 817.945(5)	−0.095	
1	99 671.421(5)	−0.122			99 755.390(5)	−0.123	
2	99 463.573(5)	−0.094			99 603.037(5)	−0.040	
3	99 168.359(6)	−0.122			99 362.672(6)	−0.119	
				(9,0)			
0					100 869.606(5)	−0.054	
1	100 724.240(5)	−0.043			100 804.788(5)	−0.075	
2					100 649.125(9)	−0.012	
3					100 404.350(20)	−0.061	
				(10,0)			
0					101 891.233(5)	−0.057	
1	101 746.444(5)	−0.149	-0.036		101 825.293(5)	−0.070	0.003
2	101 536.864(5)	−0.052			101 668.268(5)	0.022	−0.012
3	101 238.263(6)	−0.069			101 423.706(6)	−0.035	
				(11,0)			
0					102 882.115(5)	−0.045	−0.045
1	102 738.539(5)	−0.134	−0.011		102 813.729(5)	−0.074	−0.041
2	102 527.744(5)	−0.042			102 652.762(5)	−0.004	−0.078
3	102 226.698(6)	−0.073			102 401.014(6)	−0.067	
4					102 061.112(7)	−0.023	
5					101 636.453(7)	−0.137	
				(12,0)			
0					103 844.532(5)	−0.038	−0.088
1	103 701.023(5)	−0.120	−0.147		103 776.639(5)	−0.124	−0.111
2	103 490.154(5)	−0.042	−0.096		103 622.031(5)	0.005	−0.059
3	103 189.607(6)	−0.124	−0.103		103 340.273(6)	−0.118	−0.147
4					103 003.776(9)	−0.119	
5					102 576.045(9)	−0.105	
				(13,0)			
0					104 776.413(5)	−0.067	−0.077
1	104 634.440(5)	−0.113	−0.210		104 704.825(5)	−0.107	−0.045
2	104 422.041(5)	−0.065	−0.069		104 539.095(5)	−0.031	−0.035
3					104 281.088(6)	−0.123	−0.072
4	103 724.660(15)	−0.045			103 933.577(7)	−0.048	

Note: All values are given in cm^{-1}. The transition frequencies are compared with the experimental values by the Meudon group (Δ_{o-m}) (16) and by those of Hinnen et al. (Δ_{o-h}) (25).

and hence a systematic shift may be introduced.

A second accurate, but less extensive, data set is that of Hinnen et al. (25); wherever possible a comparison was made in the tables with those data as well. The previous laser-based data of Hinnen et al. (25) are found to be systematically higher by 0.07 cm^{-1}, where an experimental accuracy on the order of 0.05 cm^{-1} was estimated. A statistical analysis would again imply that there is a systematic off-set in the data of Hinnen et al. at the level of 1/4 of the line width in that experiment. We do not have an explanation for this phenomenon, other than that it may somehow be related to the procedures of comparison with the Doppler-broadened I_2-atlas (35) as a reference spectrum.

At the present level of accuracy it is not useful to attempt fitting procedures to derive effective molecular constants. A band-by-band analysis lacks sufficient data, while a global fit has to consider the non-adiabatic interactions, which cannot be dealt with at this level of accuracy. The present status of state-of-the-art close-coupling models are no better than 0.1 cm^{-1}. Calculations by the Meudon group (16–18) take into account non-adiabatic couplings between the four lowest electronic

Table 4. Observed transitions of the $B^1\Sigma_u^+ - X^1\Sigma_g^+(v',0)$ Lyman bands in H_2 for $v' = 14$–18, obtained with frequency mixing scheme II.

J	P(J)	Δ_{o-m}	Δ_{o-h}	Band	R(J)	Δ_{o-m}	Δ_{o-h}
				(14,0)			
0					105 689.330(11)	−0.020	−0.020
1	105 539.334(11)	−0.149	−0.056		105 598.807(11)	−0.036	−0.123
				(15,0)			
0					106 556.671(11)	−0.029	−0.019
1	106 416.181(11)	−0.082	−0.009		106 482.187(11)	−0.076	−0.030
				(16,0)			
0					107 404.159(11)	−0.001	−0.011
1	107 265.499(11)	−0.084	−0.001		107 326.898(11)	−0.065	−0.052
2					107 153.562(11)	−0.015	0.002
				(17,0)			
0					108 226.909(11)	−0.051	−0.111
1	108 087.714(11)	−0.029	−0.046		108 149.818(11)	−0.005	−0.122
				(18,0)			
0					109 021.296(11)	0.006	−0.124
1	108 883.440(11)	−0.133	−0.120		108 941.732(11)	−0.111	−0.078
2					108 764.439(11)	−0.048	−0.071

Note: All values are given in cm^{-1}. The transition energies are compared with the experimental values of the Meudon group (Δ_{o-m}) (16) and those of Hinnen et al. (Δ_{o-h}) (25).

Table 5. Observed transitions of the $C^1\Pi_u - X^1\Sigma_g^+(v',0)$ Werner bands in H_2 for $v' = 0$–3, obtained with frequency mixing scheme I.

J	P(J)	Δ_{o-m}	Δ_{o-h}	Q(J)	Δ_{o-m}	Δ_{o-h}	R(J)	Δ_{o-m}	Δ_{o-h}
(0-0) Band									
0							99 152.060(5)	−0.020	
1				99 032.367(5)	−0.186		99 157.343(5)	−0.090	
2	98 797.689(6)	−0.018		98 917.991(6)	0.044		99 105.580(6)	−0.047	
3	98 570.314(6)	−0.087		98 747.918(6)	−0.013		98 997.134(6)	0.013	
(1-0) Band									
0							101 457.569(5)	0.039	
1				101 337.862(5)	−0.221		101 456.482(5)	−0.091	
2	101 103.199(6)	0.042		101 217.192(6)	−0.015		101 394.780(6)	−0.047	
3	100 869.448(8)	−0.093		101 037.729(8)	−0.072		101 271.091(9)	−0.150	
(2-0) Band									
0							103 628.662(5)	−0.098	−0.088
1				103 509.373(5)	−0.110	−0.117	103 619.976(5)	−0.137	−0.064
2	103 274.289(6)	−0.098	−0.151	103 382.564(5)	−0.123	−0.086	103 541.589(6)	−0.098	−0.091
3	103 032.948(7)	−0.133		103 193.933(7)	−0.118	−0.107	103 436.111(7)	−0.110	−0.049
4	102 727.166(7)	−0.096		102 945.305(7)	−0.037				
5				102 639.037(8)	−0.134				
(3-0) Band									
0							105 660.712(5)	−0.028	−0.088
1				105 549.599(5)	−0.074	−0.131	105 665.270(5)	−0.083	−0.110
2	105 306.339(5)	−0.028	−0.061	105 416.752(5)	−0.015	−0.058	105 584.168(5)	−0.009	−0.092
3	105 078.236(6)	0.085	−0.104	105 219.106(6)	−0.135	−0.094	105 438.556(6)	−0.025	−0.084
4							105 228.227(6)	−0.055	

Note: All values are given in cm^{-1}. The values between parentheses are the uncertainties of the last digits. The transition energies are compared with the values of the Meudon group (Δ_{o-m}) (16) and those of Hinnen et al. (Δ_{o-h}) (25).

states of singlet character and u-symmetry. Such calculations have been refined since the publication of refs. 16, 17, but the improvements have not led to changes in level energies or transition frequencies, but rather in line strengths. We note here that the present study only produces accurate line positions. In a $1 + 1'$ photo-ionization study only relative intensities are measured that largely depend on the wavelength and intensity of the UV laser probing the ionization continuum. Hence, the ob-

Table 6. Observed transitions of the $C^1\Pi_u - X^1\Sigma_g^+(v', 0)$ Werner bands in H_2 for $v' = 4$, obtained with frequency mixing scheme II.

J	P(J)	Δ_{o-m}	Δ_{o-h}	Q(J)	Δ_{o-m}	Δ_{o-h}	R(J)	Δ_{o-m}	Δ_{o-h}
(4-0) Band									
0							107 580.936(11)	0.006	−0.014
1				107 460.201(11)	−0.072	−0.049	107 562.926(11)	−0.107	−0.064
2	107 226.569(11)	0.012	0.029	107 321.372(11)	−0.065	−0.068	107 475.203(11)	0.006	−0.037
3	106 975.891(12)	−0.142	−0.081	107 114.785(12)	−0.004	0.015	107 317.820(12)	−0.061	0.010

Note: All values are given in cm^{-1}. The values between parentheses are the uncertainties of the last digits. The transition frequencies are compared with those of the Meudon group (Δ_{o-m}) (16) and those of Hinnen et al. (Δ_{o-h}) (25).

served intensities do not give reliable information on the B–X line strengths.

A Dunham analysis was performed on a limited set of data with the aim of verifying the consistency of the data. In the region of excited energies below 99 000 cm^{-1}, the $B^1\Sigma_u^+$, $v' =$ 0–7 levels have no accidental perturbations with the $C^1\Pi$ state; interactions with higher lying states only cause small global shifts. Hence, in a Dunham analysis the data obtained for $B^1\Sigma_u^+$, $v' = 2$–7 were fitted to the functional form:

$$[1] \qquad E(v, J) = \sum_{k,j} Y_{k,j}(v + \frac{1}{2})^k [J(J+1)]^j$$

In total, 26 rotational states were observed in these bands as listed in Tables 2 and 3. Energies of the $v = 6$ band, which are measured with less accuracy, are used with reduced weight in the fit. Eleven Y_{kl} constants are determined and listed in Table 7, leaving 15 degrees of freedom for the fit. The constants have been chosen such that the sum of square deviations χ^2, divided by the number of degrees of freedom, is minimized; actually a small number of parameters could be added without a significant change, but none can be omitted. The main conclusion of this analysis is that the rovibrational structure of this part of the data set is smooth with an accuracy of 0.0135 cm^{-1}. There are no obvious drop-outs; the maximum deviation found is 0.030 cm^{-1} for $B^1\Sigma_u^+$, $v = 6$, $J = 2$, +0.023 cm^{-1} for $v = 7$, $J = 2$, and −0.021 cm^{-1} for $v = 7$, $J = 0$. We conclude further that the identification and use of specific I_2 saturation lines is unambiguous and correct for the bands in Tables 2 and 3.

Combination differences between P($J + 2$) and R(J) lines can further be verified with calculated ground state rotational splittings to test the accuracy and the internal consistency of the present data set. From the constants of Jennings et al. (36) the three lowest splittings can be calculated: 354.3734(2) cm^{-1}, 587.0325(2) cm^{-1}, and 814.4246(3) cm^{-1}. These splittings are consistent with the most accurate non-adiabatic calculations by Wolniewicz (13). The entire data set of Lyman and Werner band lines contains 11 measurements of the R(0)–P(2) energy splitting, of which the combination differences are plotted in Fig. 4. This shows the consistency of the data set involving these 22 spectral lines. The deviation of the combination differences from their average value amounts to much less than the typical uncertainties of 0.008 cm^{-1} (combined errors). This suggests that the determination of transition frequencies is more accurate than follows from the evaluation of the error budget for these pairs of lines. A statistical analysis yields a value for the combination difference of 354.3720(23) cm^{-1}, in agreement with the IR data (36). A similar procedure can be performed for the R(1)–P(3) combination differences where an average value of 587.031(3) cm^{-1} is derived from a set of nine pairs. The statistics are shown in Fig. 5. For the next combination difference, between R(2) and P(4) lines there are only two observations, in the B–X(13, 0) and C–X(2, 0) bands, yielding an average value of 814.426(8) cm^{-1}, which is in perfect agreement with the IR data (36).

Table 7. Dunham coefficients Y_{kl} representing the energies of observed rovibrational $B^1\Sigma_u^+$, $v = 2$–7 states, all values in cm^{-1}.

Y_{00}	89 533.70
Y_{10}	1352.907
Y_{20}	−18.4749
Y_{30}	0.1914
Y_{40}	−0.005075
Y_{01}	19.8673
Y_{11}	−1.0224
Y_{21}	0.06165
Y_{31}	−0.002808
Y_{02}	−0.01391
Y_{12}	0.000933

Note: The root mean square deviation of the representation from experimental energies is 0.0135 cm^{-1}.

On the basis of the ground state rotational energy splittings, accurately known from ref. 36, a number of transition frequencies for P-lines can be calculated, therewith extending the data set of Lyman and Werner bands spectral lines. Apart from the three lowest splittings cited above, we adopt values for higher lying combination differences: $\Delta_{53} = 1034.6703(1)$ cm^{-1}, $\Delta_{64} = 1246.098(1)$ cm^{-1}, and $\Delta_{75} = 1447.279(2)$ cm^{-1}. The calculated transition frequencies for the 60 P-lines and their estimated uncertainties are listed in Table 8.

The presently obtained data, measured at a greatly improved accuracy, provide a challenging test ground for future ab initio and close-coupling calculations. The accurately determined $B^1\Sigma_u^+$, v, J excited state level energies can be employed in multiple resonance studies to also determine accurate level energies of higher lying electronic states in H_2 as was demonstrated for some states of g symmetry by de Lange et al. (37). Also, the values can be incorporated in existing data sets on transitions between excited states to derive level energies of improved accuracy. One such example is that of the bound energy levels just below the $n = 2$ dissociation threshold in

Fig. 4. Combination differences between 11 sets of R(0) and P(2) lines measured in a number of Lyman and Werner bands. Indicated are the (weighted) average value from the 11 pairs and the resulting uncertainty: 354.3720(23) cm^{-1}.

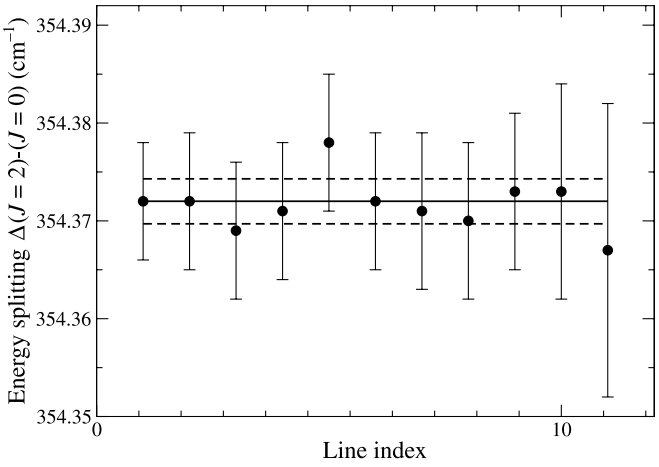

Fig. 5. Combination differences between nine sets of R(1) and P(3) lines measured in a number of Lyman and Werner bands. Indicated are the (weighted) average value and resulting uncertainty: 587.031(3) cm^{-1}.

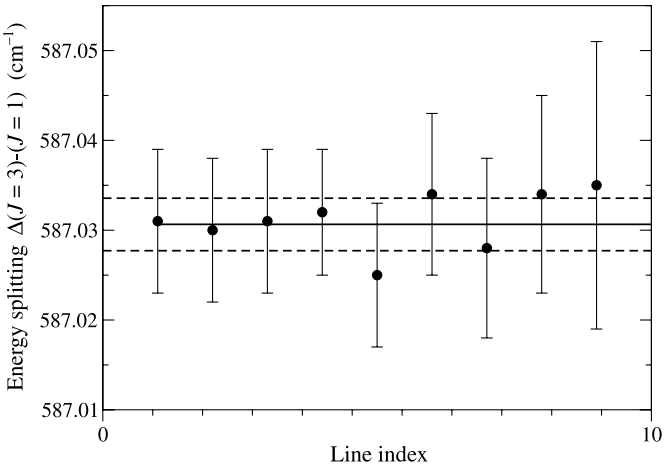

H_2 (38). Combination with the present data on the $B^1\Sigma_u^+$, $v = 14$, $J = 0$ level energies yields improved values for level energies in the $II'^1\Pi_g$ potential: 118 361.202(13) cm^{-1} for the $II'^1\Pi_g$, $v = 2$, $J = 1(e)$ level, 118 373.169(13) cm^{-1} for the $II'^1\Pi_g$, $v = 3$, $J = 1(e)$ level, and 118 376.618(16) cm^{-1} for the $II'^1\Pi_g$, $v = 4$, $J = 1(e)$ level. The assignment of the latter two levels is tentative.

The accurate zero-velocity line centers form a set of lines for deducing accurate velocities of astrophysical objects, when ultra-high-resolution XUV spectrometers are used aboard satellites. At temperatures of 10 K the FWHM-Doppler width of the H_2 lines is 4.5 GHz; this may be compared with the width (0.55 GHz) and accuracy (<0.3 GHz) obtained in the present laboratory investigation. Finally, the present data may be implemented in improved comparisons between laboratory data and observed spectra from distant quasars, thus revealing possible cosmological variations of the proton-to-electron mass ratio (39–41).

Table 8. Calculated transition frequencies of some Lyman (L) and Werner (W) P-lines via the accurately known ground state energies.

Line	ν_0	Line	ν_0
L 2-0 P(2)	92 484.178 (4)	L 2-0 P(3)	92 203.261 (4)
L 2-0 P(4)	91 844.667 (4)	L 3-0 P(3)	93 445.641 (4)
L 3-0 P(4)	93 082.746 (4)	L 3-0 P(5)	93 644.027 (4)
L 4-0 P(2)	94 941.132 (4)	L 4-0 P(3)	94 654.713 (4)
L 4-0 P(4)	94 287.939 (4)	L 4-0 P(5)	93 844.142 (4)
L 5-0 P(2)	96 119.897 (4)	L 5-0 P(3)	95 831.044 (4)
L 5-0 P(4)	95 460.666 (4)	L 5-0 P(5)	95 012.147 (4)
L 6-0 P(2)	97 266.227 (8)	L 6-0 P(3)	96 975.095 (8)
L 7-0 P(2)	98 380.534 (5)	L 7-0 P(3)	98 087.083 (5)
L 7-0 P(4)	97 709.990 (6)	L 8-0 P(4)	98 788.612 (5)
L 8-0 P(5)	98 328.002 (6)	L 9-0 P(2)	100 515.233 (5)
L 9-0 P(3)	100 217.756 (5)	L 9-0 P(4)	99 834.700 (9)
L 9-0 P(5)	99 369.680 (20)	L 10-0 P(4)	100 853.843 (5)
L 10-0 P(5)	100 389.036 (6)	L 11-0 P(4)	101 838.337 (5)
L 11-0 P(5)	101 366.344 (6)	L 11-0 P(6)	100 815.014 (7)
L 11-0 P(7)	100 189.174 (7)	L 12-0 P(4)	102 807.606 (5)
L 12-0 P(5)	102 305.603 (6)	L 12-0 P(6)	101 757.678 (9)
L 12-0 P(7)	101 128.766 (9)	L 13-0 P(3)	104 117.793 (5)
L 13-0 P(5)	103 246.418 (6)	L 13-0 P(6)	102 687.479 (8)
L 14-0 P(2)	105 334.957 (11)	L 14-0 P(3)	105 011.775 (11)
L 15-0 P(2)	106 202.298 (11)	L 15-0 P(3)	105 895.155 (11)
L 16-0 P(2)	107 049.786 (11)	L 16-0 P(3)	106 739.866 (11)
L 16-0 P(4)	106 339.137 (11)	L 17-0 P(2)	107 872.536 (11)
L 17-0 P(3)	107 562.786 (11)	L 18-0 P(2)	108 666.923 (11)
L 18-0 P(3)	108 354.700 (11)	L 18-0 P(4)	107 950.014 (11)
W 0-0 P(4)	98 291.155 (6)	W 0-0 P(5)	97 962.464 (6)
W 1-0 P(4)	100 580.355 (6)	W 1-0 P(5)	100 236.421 (9)
W 2-0 P(5)	102 401.441 (7)	W 3-0 P(4)	104 769.743 (5)
W 3-0 P(5)	104 403.886 (6)	W 3-0 P(6)	103 982.129 (6)
W 4-0 P(4)	106 660.778 (11)	W 4-0 P(5)	106 283.150 (12)

Notes: Values in cm^{-1}.

Acknowledgments

The authors acknowledge the Netherlands Foundation for Fundamental Research of Matter (FOM) for financial support. The work was also supported by the European Union via the RTN network on Reactive Intermediates (HPRN-CT-2000-00006); ER acknowledges the EU for a Marie Curie individual fellowship (HPMF-CT-2000-00964). Additionally this work was supported by the European Community - Access to Research Infrastructures action of the Improving Human Potential Programme, Contract No. HPRI-CT-1999-00064.

References

1. T. Lyman. Astrophys. J. **19**, 263 (1904).
2. T. Lyman. Astrophys. J. **23**, 181 (1906).
3. S. Werner Proc. R. Soc. London Ser. A, **113**, 107 (1926).
4. G. Herzberg. Nature (London), **163**, 170 (1949).
5. G. Herzberg and Ch. Jungen. J. Mol. Spectrosc. **41**, 425 (1972).

6. G. Herzberg. J. Mol. Spectrosc. **33**, 147 (1970).
7. Ch. Jungen, I. Dabrowski, G. Herzberg, and M. Vervloet. J. Chem. Phys. **93**, 2289 (1990).
8. G. Herzberg and L.L. Howe. Can. J. Phys. **37**, 636 (1959).
9. I. Dabrowski and G. Herzberg. Can. J. Phys. **52**, 1110 (1974).
10. T. Namioka. J. Chem. Phys. **40**, 3154 (1964).
11. I. Dabrowski. Can. J. Phys. **62**, 1639 (1984).
12. J.-Y. Roncin and F. Launay. J. Phys. Chem. Ref. Data, Monograph 4 (1994).
13. L. Wolniewicz. J. Chem. Phys. **103**, 1792 (1995).
14. W. Cencek, J. Komasa, and J. Rychlewski. Chem. Phys. Lett. **246**, 417 (1995).
15. L. Wolniewicz. Chem. Phys. Lett. **233**, 644 (1995).
16. H. Abgrall, E. Roueff, F. Launay, J.-Y. Roncin, and J.-L. Subtil. J. Mol. Spectrosc. **157**, 512 (1993).
17. H. Abgrall, E. Roueff, F. Launay, J.-Y. Roncin, and J.-L. Subtil. Astron. Astrophys. Suppl. Ser. **101**, 273 (1993).
18. H. Abgrall, E. Roueff, F. Launay, J.-Y. Roncin, and J.-L. Subtil. Astron. Astrophys. Suppl. Ser. **101**, 323 (1993).
19. G.C. Carruthers. Astrophys. J. **161**, L81 (1970).
20. D.C. Morton and H.L. Dinerstein. Astrophys. J. **204**, 1 (1976).
21. S.R. Federman, J.A. Cardelli, E.F. van Dishoeck, D.L. Lambert, and J.H. Black. Astrophys. J. **445**, 325 (1995).
22. J. Ajello, D. Shemansky, W. Pryor, K. Tobiska, C. Hord, S. Stephens, I. Stewart, J. Clarke, K. Simmons, W. McClintock, C. Barth, J. Gebben, D. Miller, and B. Sandel. J. Geophys. Res. E, **103**, 20 125 (1998).
23. H.W. Moos, W.C. Cash, L.L. Cowie, A.F. Davidsen, A.K. Dupree, P.D. Feldman, S.D. Friedman, J.C. Green, R.F. Green, C. Gry, J.B. Hutchings, E.B. Jenkins, J.L. Linsky, R.F. Malina, A.G. Michalitsianos, B.D. Savage, J.M. Shull, O.H.W. Siegmund, T.P. Snow, G. Sonneborn, A. Vidal-Madjar, A.J. Willis, B.E. Woodgate, D.G. York, T.B. Ake, B.-G. Andersson, J.P. Andrews, R.H. Barkhouser, L. Bianchi, W.P. Blair, K.R. Brownsberger, A.N. Cha, P. Chayer, S.J. Conard, A.W. Fullerton, G.A. Gaines, R. Grange, M.A. Gummin, G. Hebrard, G.A. Kriss, J.W. Kruk, D. Mark, D.K. McCarthy, C.L. Morbey, R. Murowinski, E.M. Murphy, W.R. Oegerle, R.G. Ohl, C. Oliveira, S.N. Osterman, D.J. Sahnow, M. Saisse, K.R. Sembach, H.A. Weaver, B.Y. Welsh, E. Wilkinson, and W. Zheng. Astrophys. J. **538**, L1 (2000).
24. P.C. Hinnen, W. Hogervorst, S. Stolte, and W. Ubachs. Appl. Phys. B, **59**, 307 (1993).
25. P.C. Hinnen, W. Hogervorst, S. Stolte, and W. Ubachs. Can. J. Phys. **72**, 1032 (1994).
26. E. Reinhold, W. Hogervorst, and W. Ubachs J. Mol. Spectrosc. **180**, 156 (1996).
27. K.S.E. Eikema, W. Ubachs, W. Vassen, and W. Hogervorst. Phys. Rev. **A55**, 1866 (1997).
28. W. Ubachs, K.S.E. Eikema, W. Hogervorst, and P.C. Cacciani, J. Opt. Soc. Am. **B14**, 2469 (1997).
29. I. Velchev, R. van Dierendonck, W. Hogervorst, and W. Ubachs. J. Mol. Spectrosc. **187**, 21 (1998).
30. S.C. Xu, R. van Dierendonck, W. Hogervorst, and W. Ubachs, J. Mol. Spectrosc. **201**, 256 (2000).
31. J. Philip, J.P. Sprengers, P. Cacciani, C.A. de Lange, and W. Ubachs. Appl. Phys. B, **78**, 737 (2004).
32. D. Wetzig, A.D. Rudert, and H. Zacharias. Eur. J. Phys. D**17**, 181 (2001).
33. J. Rychlewski, J. Komasa, and W. Cencek. Phys. Rev. A , **41**, 5825 (1990).
34. S. Gangopadhyay, N. Melikechi, and E.E. Eyler. J. Opt. Soc. Am. B , **11**, 231 (1994).
35. S. Gerstenkorn and P. Luc Atlas du spectre d'absorption de la molecule de l'iode entre 14800-20000 cm^{-1}. Editions du CNRS, Paris. 1978.
36. D.E. Jennings, S.L. Bragg, and J.W. Brault. Astrophys. J. **282**, L85 (1984).
37. A. de Lange, E. Reinhold, and W. Ubachs. Phys. Rev. A , **65**, 064 501 (2002).
38. Th.G.P. Pielage, A. de Lange, F. Brandi, and W. Ubachs. Chem. Phys. Lett. **366**, 583 (2002).
39. D.A. Varshalovich and S.A. Levshakov. JETP Lett. **58**, 237 (1993).
40. A.Y. Pothekhin, A.V. Ivanchik, D.A. Varshalovich, K.M. Lanzetta, J.A. Baldwin, G.M. Williger, and R.F. Carswell. Astrophys. J. **505**, 523 (1998).
41. W. Ubachs and E. Reinhold. Phys. Rev. Lett. **92**, 101 302 (2004).